

Article

The Role of Fluid Overpressure on the Fracture Slip Mechanism Based on Laboratory Tests That Stimulating Reservoir-Induced Seismicity

Yujie Zhu ^{1,2}, Chen Xu ^{1,3,*}, Danqing Song ¹, Xiaoli Liu ¹  and Enzhi Wang ¹¹ State Key Laboratory of Hydrosience and Engineering, Tsinghua University, Beijing 100084, China² Key Laboratory of Geotechnical Mechanics and Engineering of Ministry of Water Resources, Changjiang River Scientific Research Institute, Wuhan 430010, China³ Changjiang Institute of Survey Planning Design and Research, Wuhan 430010, China

* Correspondence: xuchen_office@163.com

Abstract: A critically stressed fracture will slide in response to the increase in fluid pressure inside the fracture while impounding, which will trigger induced seismicity. The mechanism of fluid overpressure is regarded as a significant factor in the reaction of the fracture slip after water diffusing. This study uses a shearing test with a cylinder of granite, with 100 mm height and 50 mm diameter, under the condition of hydraulic-mechanic (HM) coupling to figure out how fluid overpressure alters the mechanical behavior of the critically stressed fracture. The cyclic water pressurization simulates periodical impounding in the water reservoir. Results show that several slip events happen when water pressure continues to rise higher than the stable state. The change of roughness also indicates the deterioration of the fracture surface while sliding. According to the results, we conclude that the difference between inlet pressure and outlet pressure leads to an overpressure of the fracture, promoting a series of slips and induced seismicity. Hydraulic energy is introduced to explain the relationship between the input and output energy, which is also strong evidence to illustrate that fluid overpressure is a crucial mechanism in reservoir-induced seismicity.



Citation: Zhu, Y.; Xu, C.; Song, D.; Liu, X.; Wang, E. The Role of Fluid Overpressure on the Fracture Slip Mechanism Based on Laboratory Tests That Stimulating Reservoir-Induced Seismicity. *Appl. Sci.* **2023**, *13*, 3382. <https://doi.org/10.3390/app13063382>

Academic Editors: Hu Li, Ahmed E. Radwan and Shuai Yin

Received: 9 February 2023

Revised: 4 March 2023

Accepted: 5 March 2023

Published: 7 March 2023



Copyright: © 2023 by the authors. Licensee MDPI, Basel, Switzerland. This article is an open access article distributed under the terms and conditions of the Creative Commons Attribution (CC BY) license (<https://creativecommons.org/licenses/by/4.0/>).

Keywords: reservoir-induced seismicity; shearing test; overpressure; hydraulic energy

1. Introduction

Reservoir-induced seismicity is an interesting area of research because there are still many challenges in figuring out how seismicity is triggered and how long it lasts. Fractures divide the rock mass into discontinuity and may control mechanistic behavior under certain conditions, which is one of the main reasons for inducing seismicity and slope sliding. In North Dakota, earthquakes are induced by the interaction of hydraulic fractures with large faults in the region [1]. Induced earthquakes are particularly pronounced in Oklahoma and Kansas, where studies have shown that the underground storage of salt water is the primary cause [2]. A bimodal distribution of fluid injection-induced microseisms was observed in 2012 at the Newberry Volcano Enhanced Geothermal (EGS) Demonstration Project in Oregon, USA. EGS presents challenges for enhancing permeability and reducing instability [3].

Especially near the water reservoir, the seepage field would change significantly due to impoundment. Critically stressed fractures are expected to be unstable since the original balance has been broken when considering the coupling influence between the liquid phase and the solid phase. Therefore, the slight disturbance of water pressure can crucially alter the state of a fracture. Particularly, fluid overpressure inside the fracture takes an obvious part in reactivating a fracture and releasing energy.

Evidence shows that fluid overpressure is a significant factor in the nucleation and propagation of ruptures [4]. The maximum fluid overpressure could be predicted and

controlled using tectonic stress and fracture orientation [5]. Changes in the stress state are accompanied by fluid redistribution and are ensured by the critical interdependence of differential stress and sustainable overpressure [6]. Fluid overpressure is commonly regarded as the reason for weak subduction plate boundaries [7]. The increase of fluid pressure first causes an accelerated seismic creep and fault opening; with the further increase of fluid pressure, the friction rate increases, which is conducive to seismic creep [8]. Besides, overpressure can reduce the effective overburden stress and the available stress, and can lead to under-consolidated sediment sequences, resulting in the unstable sliding of the slope and the induction of earthquake shaking [9]. Therefore, fluid overpressure is comprehensively discussed, since it is a hydrodynamic phenomenon. The fluid expansion mechanism and disequilibrium compaction mechanism are two categories used to explain the generation of overpressure [10]. Experimental analysis shows that pore pressure can be predicted based on elastic parameters [11]. The Mohr-Coulomb criterion can judge when the fractures fail, but cannot predict the mechanical behavior after the fractures break. Therefore, the energy budget is carried out to describe the input energy and output energy. The input energy equals the output energy, according to the Law of conservation of energy. Thus, the input energy, including the hydraulic energy and mechanic energy, is supposed to produce the same value of output energy, composed of friction energy, radiated energy, deformation energy and energy loss. This budget provides support to verify the role of fluid overpressure in inducing fracture sliding.

As for the water reservoir, the alteration of the underground water level is usually delayed after the modification of the reservoir impounding, indicating that the overpressure of the fracture seepage might be caused by both mechanisms. This study concentrates on the fluid expansion mechanism. However, overpressure is usually described qualitatively in macro-geology. There are a few micro descriptions that can explain this mechanism explicitly. To reveal the mechanism of activating a stressed fracture, a shearing test, based on HM coupling, is adopted to concentrate on how the overpressure activates the sliding and discusses the relationship between the input hydraulic energy and output seismic energy.

The remainder of this paper is organized as follows. Section 2 describes the experimental methodology; including setup, sample preparation and procedure. The results of the surface scanning and HM shearing test are presented in Section 3. Section 4 discusses the overpressure of the fracture reactivation and energy budget. Section 5 concludes this article.

This paper aims to discuss how fluid overpressure induces seismicity when the fracture is critically stressed. The HM coupling experiment shows that the unstable slip of fracture is driven by the inlet pressure and outlet pressure. Seismic events imply that unstable sliding happens, which occurs at the moment the fluid pressure rises over the threshold pressure. This paper compares the overpressure and understress states of the fracture to illustrate the mechanism of reservoir-induced seismicity. In addition, hydraulic energy is analyzed to explain how fluid overpressure can induce unstable sliding by establishing the relationship between the input energy and released energy, which is also an effective method for predicting the magnitude and total released energy.

2. Materials and Methods

2.1. Setup and Sample Preparation

Granite is used for this research, which is composed of quartz, feldspar and hornblende (as shown in Figure 1). The bulk density is 2610 kg/m^3 with a Young's modulus of 84 GPa and a Poisson's ratio of 0.25. A cylinder sample, with 100 mm height and 50 mm diameter, is separated smoothly along the surface with a 30° inclination to the vertical axis to simulate a pre-existing fracture. Then the fracture is refined with sandpaper with particles of $18.3 \mu\text{m}$. Two boreholes are drilled parallel to the vertical axis near the fracture surface, allowing the fluid to be distributed in the fracture during the tests.

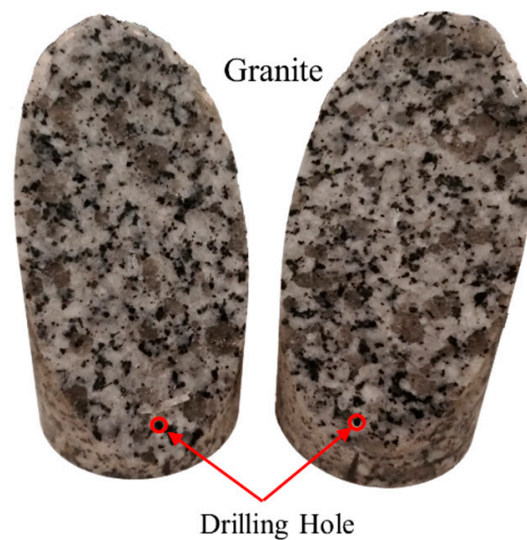


Figure 1. A granite sample with a 30° inclination to the vertical axis.

The schematic of the HM-coupling shearing test is shown in Figure 2. The assembled sample is placed in the triaxial cell, fixed by the core holder. The oil tank provides confining pressure and the water tank supplies the upstream pressure during tests. A Teflon jacket is used to isolate the sample from the confining oil and assures that the water is sealed inside the sample to prevent the mixing of the water and oil. The process of loading and water pressurization is controlled and recorded by the controller. In addition, the monitoring system will record the parameters of the downstream pump, including the flow pressure and flow rate.

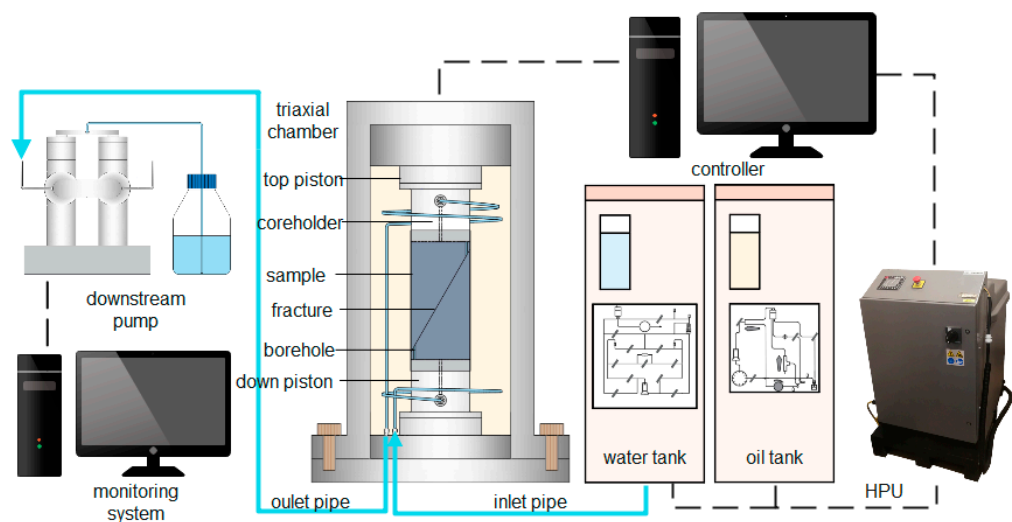


Figure 2. A schematic of the HM-coupling shearing test.

2.2. Experimental Procedure

After assembling the sample in the triaxial cell, the confining pressure will be increased by the piston in the oil tank to the predefined value. Then the pore pressure inside the sample will be supplied by the water tank (shown in Figure 3). The shear strength of the pre-existing fracture is measured before each test, by compressing the sample by moving the axial piston at a constant rate of 1 $\mu\text{m/s}$. The axial stress will be modified specifically to satisfy the required shear stress on the fracture.

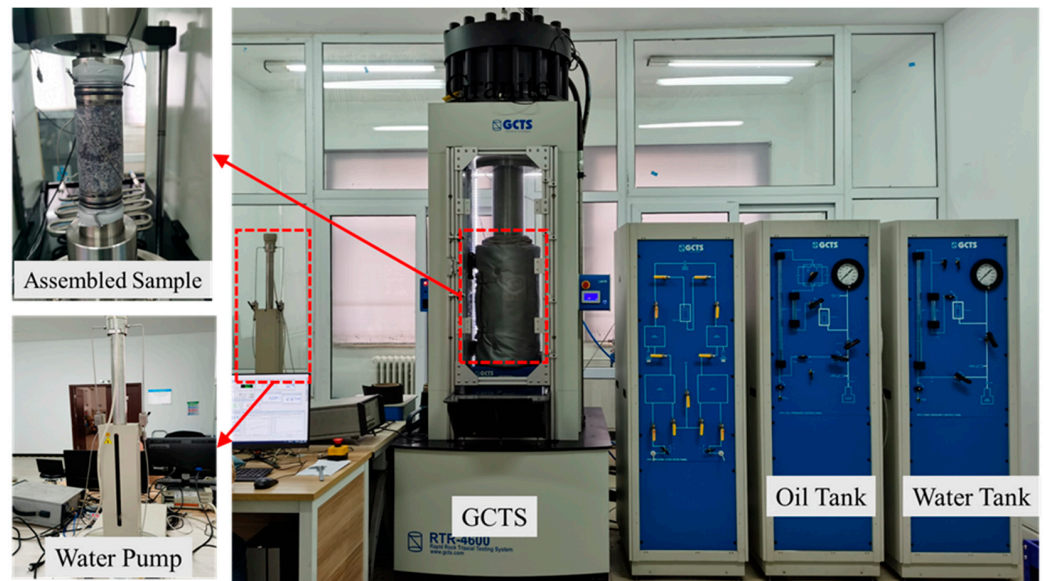


Figure 3. The experimental setup of the HM-coupling shearing test.

Cyclic pressurization is applied during the test to simulate the cyclic impounding process of a water reservoir. Figure 4 shows the alteration of the inlet pressures because the inlet pressure is a typical curve for water reservoirs, such as Xiluodu Reservoir and Three Gorge Reservoir. Each cycle has four steps corresponding to the real oscillation of a reservoir: rising water level, high level, drawdown, and low water level. The water pressure is increasing and decreasing at a constant rate of 0.005 MPa/s to simplify the simulating model. This rate is adopted because it is slow enough not to cause excessive pressure concentration around the inlet hole while being fast enough to quickly simulate the process of reservoir impoundment. The whole process has 8 cycles, divided into 3 stages, shown in Figure 4. The grey part shows the first impounding stage, requiring a relatively low water level that causes the inlet pressure to rise from 5 to 6 MPa in 200 s and maintains this for 300 s before falling to 5.5 MPa. The light red part represents the second stage, including two cycles during which the water pressure raises to 7 MPa and reduces to 6 MPa. The blue part represents the third stage, assuming that the reservoir operates in a normal state, and causes the water pressure to oscillate between 7 and 8 MPa.

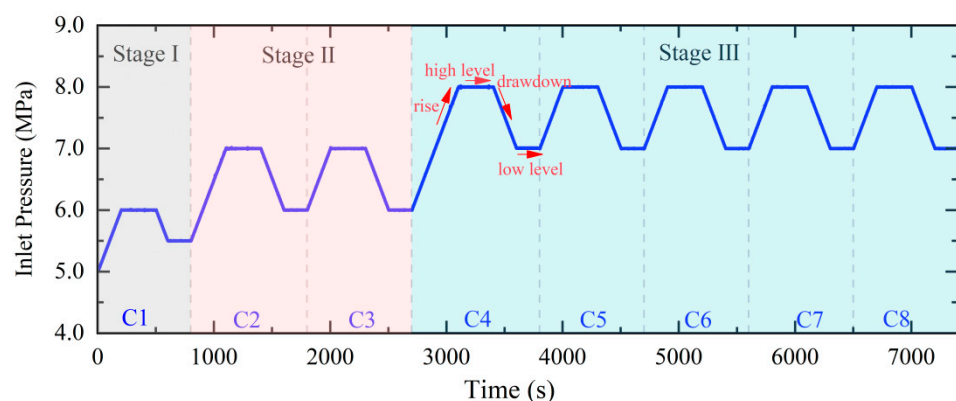


Figure 4. A schematic of the cyclic pressurization process.

3. Results

3.1. Roughness Alteration

Before the shearing test, the fracture surface of each sample is scanned to examine the evolution of the fracture after the process. Before the experiments, the fracture surface

is polished and scanned to record the root mean square (RMS) of the fractures. The RMS is used to represent the roughness of the fracture surface. When the RMS is larger, it represents a greater roughness of the surface. Figure 5a shows that the fault surface is quite smooth after polishing. Only the upper surface is shown in this article, due to the upper surface and lower surface being mirror images of each other. Before the shearing test, the root mean square is 0.6575. After the shearing test, an unstable slip occurs that will damage the fracture surface. Figure 5b shows that the RMS of the fracture surface changes to 0.7175 after shearing. This means that the roughness increases. In addition, broken minerals are discovered inside the fracture. Figure 5c represents the shear surface calculated using Figure 5a,b. The shear surface shows the sheared thickness of the fracture. This phenomenon indicates that the fracture surface is damaged during the process while the pore pressure increases to trigger the slip.

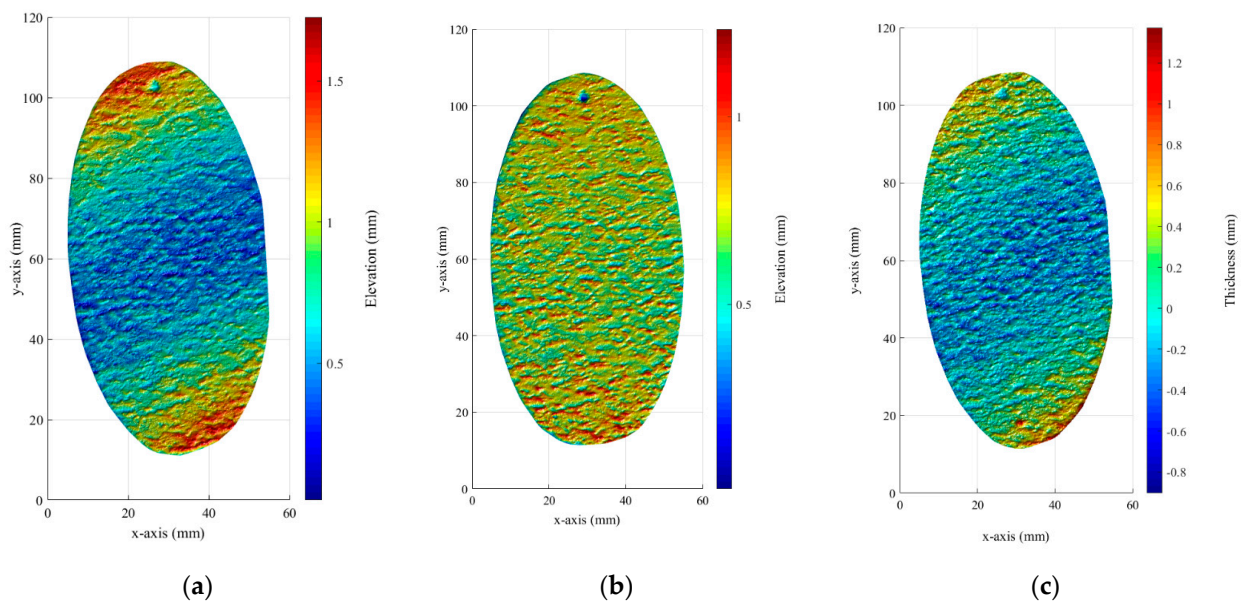


Figure 5. The contour of the roughness of the smooth fracture surface. (a) before shearing; (b) after shearing; (c) shear surface.

3.2. Mechanic Behavior of Fracture While Water Pressurization

The fracture is expected to slide during water pressurization while the normal stress on the surface remains constant so that the servo-control system can modify the confining pressure and the axial stress simultaneously. The shear stress (τ) and normal stress (σ_n) of the fracture are determined by the axial stress (σ_1) and confining pressure (σ_3):

$$\sigma_n = \frac{1}{2}[(\sigma_1 + \sigma_3) + (\sigma_1 - \sigma_3) \cos 2\theta] \quad (1)$$

$$\tau = \frac{1}{2}(\sigma_1 - \sigma_3) \sin 2\theta \quad (2)$$

where θ is the normal angle of the fracture surface, equaling 60° in this experiment. Shear displacement (D) can be calculated according to axial displacement instead of direct measurement. The initial pore pressure inside the fracture is p . Therefore, the friction coefficient (μ) is the ratio between shear strength (τ_c) and the effective normal stress ($\sigma_n - p$). r_τ is defined as the ratio between the shear stress and shear strength of the fracture while under water pressurization [12].

Since the fracture slip can release elastic energy and induce seismicity, we introduced the moment M_0 to describe the energy released while sliding. M_0 is the product of the

fracture area (A), shear displacement (D) and shear modulus (G), determined by the Young's modulus and Poisson ratio.

$$M_0 = GAD \tag{3}$$

$$M_W = \frac{2}{3} \log M_0 - 6.07 \tag{4}$$

Figure 6 shows that the fracture is pressurized at 20.8 MPa under normal stress and 13.6 MPa under shear stress. The friction coefficient is 0.87, and the ratio r_τ is 98%. The outlet pressure rises at a nonlinear incremental rate, depending on the water pressure diffusion along the fracture. There are 23 seismic events during the process.

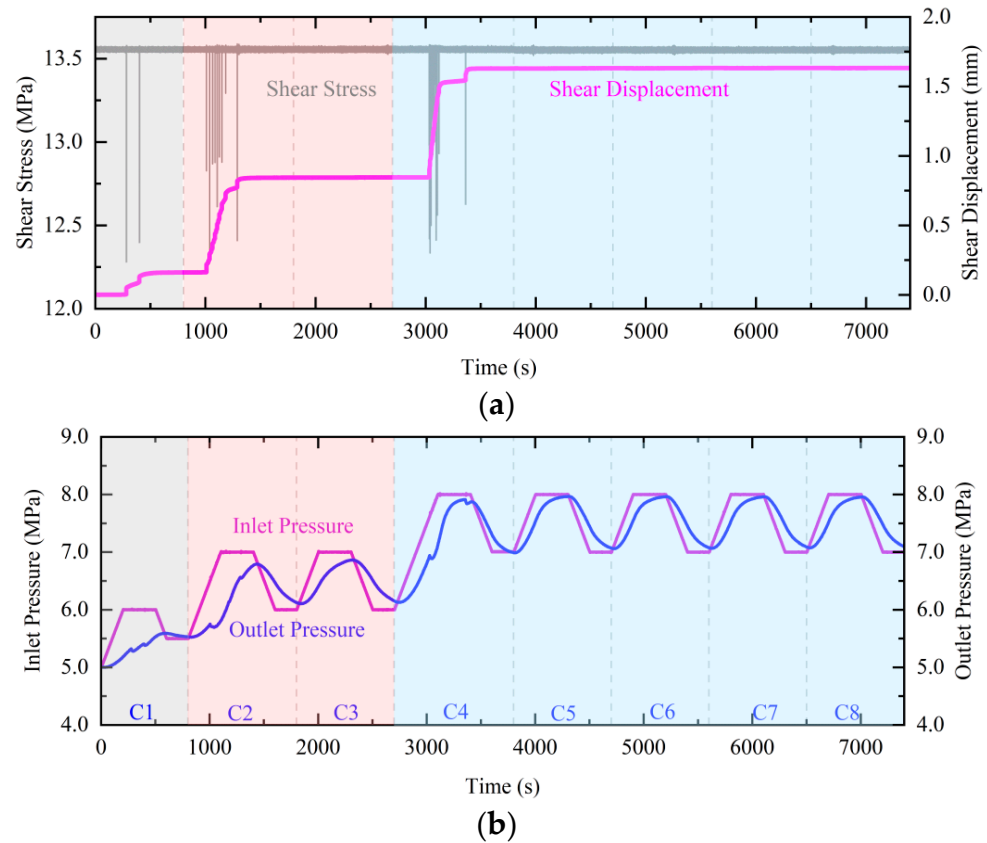


Figure 6. The cyclic pressurization instability of a saw-cut fracture. (a) The shear stress and shear displacement with shearing time; (b) The inlet pressure and outlet pressure with shearing time.

The fault failure is expected when the water pressure exceeds 5.2 MPa, due to r_τ . This happens when the outlet pressure reaches this level, meaning that the distribution of the pore pressure on the whole fault surface is over 5.2 MPa.

In the first cycle, the inlet pressure is maintained at 6.0 MPa, and the outlet pressure continuously increases. The fracture permeability before the fracture slip is 7.23 mD, which is measured based on the constant inlet pressure and increasing outlet pressure. At 282 s, when the outlet pressure reaches 5.30 MPa, the fracture slip occurs, accompanied by a shear stress drop and shear displacement jump. The outlet pressure drops immediately after the slip event because of the shear dilation of the fracture [13]. However, after two stick slips, the outlet pressure still increases due to the imbalance between the inlet and outlet pressures. At the end of the first cycle, the outlet pressure is approximately equal to the inlet pressure. This fault is transitioning from stick-slip to stable sliding.

In the second cycle, the occurrence of the slip events is also accompanied by a slight drop in the outlet pressure followed by a remarkable increase until the outlet pore pressure reaches 5.5 MPa, instead of the maximum pressure (6.8 MPa), in the second pressurization stage. However, there is no slip event in the third cycle and this could be regarded as a

stable state in the second stage. After nine slip events, the fracture permeability becomes 12.06 mD, indicating permeability enhancement during the fracture slip.

In the third stage, the fault begins to slip at the time the outlet pressure exceeds the maximum water pressure in the second stage. Twelve slips occur subsequently with the rise in inlet pressure and outlet pressure. The slip events disappear when the outlet pressure reaches 7.87 MPa. The permeability rises to 16.88 mD. Meanwhile, the outlet pressure decreases as the granular gouges produced from previous slip events are likely being compacted during the stable sliding.

Each stick-slip is recorded as a seismic event. The statistic of each slip event is drawn in Figure 7. Figure 7a shows the inlet pressure and outlet pressure with the seismic event, indicating that the necessary condition for triggering the fracture slip is an increasing average pressure along the fracture surface. The distribution of the pore pressure due to permeability can occur through both the delay of outlet pressure and the difference between the inlet and outlet pressure. This is a crucial motivation in activating the unstable slip of a critically stressed fracture. Figure 7b–d show the slip distance, maximum slip rate, and stress drop with the seismic event, respectively. The fracture slides along the surface in a moment. The shear displacement will increase rapidly. Each shear distance is recorded in Figure 7b. Slip rate is the ratio of shear displacement to slip time. When the fracture slides, the slip rate will rise suddenly. The maximum slip rate is recorded in Figure 7c. The shear stress will drop suddenly because the machine cannot track the movement within milliseconds, defined as a stress drop (Figure 7d). Since the inlet pressure increases periodically, the three parameters express a periodical trend.

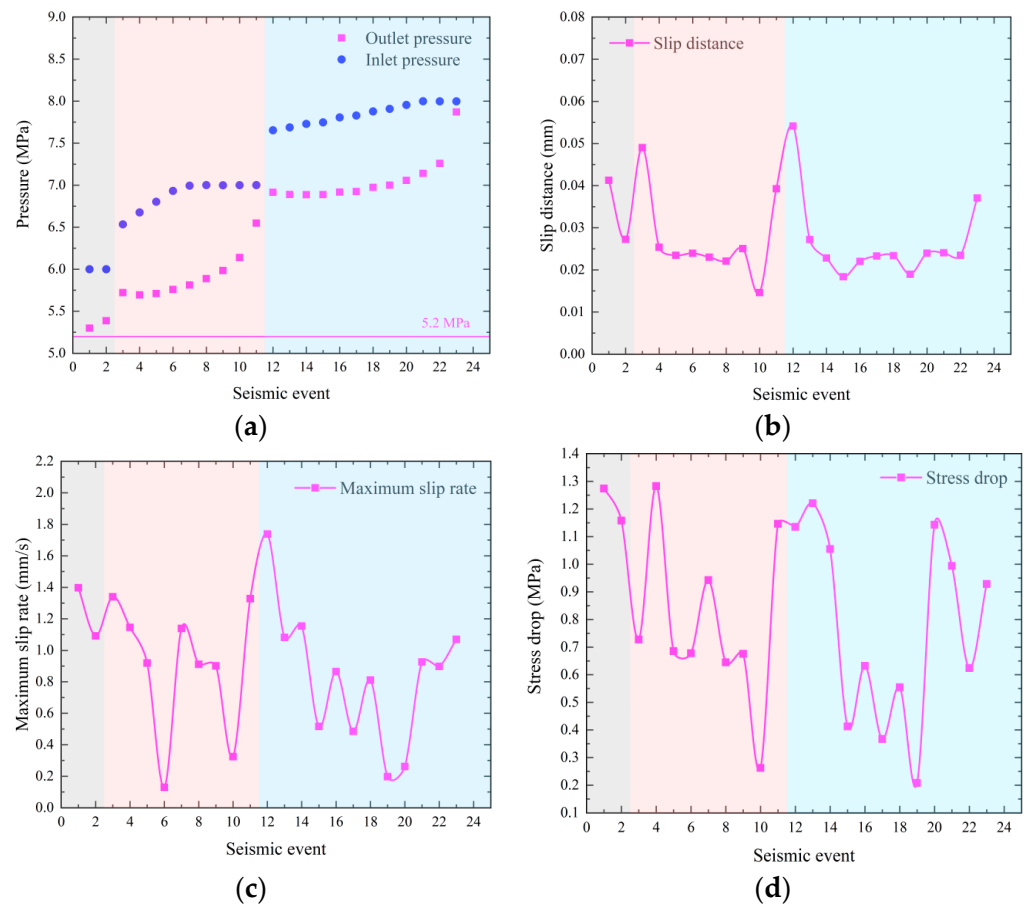


Figure 7. The dynamic slip parameters with a seismic event. (a) Pressure with a seismic event; (b) Slip distance with a seismic event; (c) Maximum slip rate with a seismic event; (d) Stress drop with a seismic event.

4. Discussion

4.1. Overpressure in Fracture Reactivation

The stimulation of triggering pre-existing fractures by cyclic water pressurization is a process of over-pressurization [6,14–17] and pore pressure diffusion [18–24] along the fracture. Each process promotes the reactivation of the pre-existing fault and induces seismicity. Overpressure is an especially crucial factor, as it controls the state of the fault. The combinations of the shear stress, normal stress, and water pressure of a fault are plotted in Figure 5, by modifying the graphical representation of Garagash [25] and Gischig [26]. According to the Mohr-Coulomb failure criterion, τ is the initial shear stress on the fault and τ_p is the shear strength acquired from the displacement-driven shear test. r_c is the ratio between shear stress (τ) and shear strength (τ_p), which is used to describe the critical state of the fault. The understress is evolved as $1 - r_c$. The fault is assumed to be critically stressed if the understress decreases to zero. On the contrary, the shear stress is 0 if the understress is equal to one. The increasing water pressure monitored by the system is defined as Δp and Δp and is normalized by the fault-effective normal stress. σ_{neff} ($\Delta p / \sigma_{neff}$) is defined to describe the overpressure of the fracture.

The diagonal in Figure 8 is a limitation in the fracture failure, dividing the fault into two states: if $\Delta p / \sigma_n < 1 - r_c$, the increased pressure and shear stress cannot induce slip; if $\Delta p / \sigma_n > 1 - r_c$, the fault is transitioning from the stable state to unstable state and an aseismic slip or seismic slip might happen. In our test, the overpressure is a dynamic oscillating state rather than a quasi-static state. Due to the heterogeneity of the pressure distribution and low permeability, the change in outlet pressure is delayed compared to the inlet pressure. Therefore, the inlet pressure and outlet pressure corresponding to every slip are analyzed in Figure 8, showing that the unstable slip occurs with the accumulation of pressure. The whole process is divided into three stages according to the inlet pressure (6 MPa, 7 MPa and 8 MPa). For each stage, the overpressure increases in both the inlet and outlet pressure. Every initiation of reactivation of the fault requires a higher pressure in both the inlet and outlet. Therefore, a higher pressure along the fault surface is a necessary condition for inducing a dynamic slip. And when a new balance between the inlet and outlet pressure has formed, the pressure-controlled stick-slip will turn into a stable sliding state. This phenomenon is consistent with the experiment investigated by Scuderi [24]. Finally, when the outlet and inlet pressure remains equal, the maximum injected energy by the rising water pressure remains constant and there is no more dynamic slip during pressure oscillation. Referring to the theory for describing the criterion of fault stability by combining the elastic dislocation theory with the rate-and-state-friction (RSF) constitutive, a relationship between fault stiffness (k_c) and effective normal stress (σ_{neff}) is defined as Equation (5). D_c is the critical slip distance for the friction of the fracture surface changing from static friction to dynamical friction. Parameter a is the fracture friction at velocity V_1 . Parameter b is the fracture friction at velocity V_2 . σ_{neff} is the effective normal stress on the fracture. All the parameters can be measured in the rate and state law friction test.

$$k_c = \frac{\sigma_{neff}(b - a)}{D_c} \quad (5)$$

where $(b - a) / D_c$ is the friction weakening rate parameter [27,28]. Equation (5) shows that increasing the pressure inside the fault can reduce k_c and promote stable sliding, rather than an earthquake slip. But seismological observations contrast with this prediction. The dynamic slip instabilities are determined by the fluid pressurization exceeding the critical stress state for reactivation. This process is driven by energy unbalance due to the decrease in effective normal stress [24].

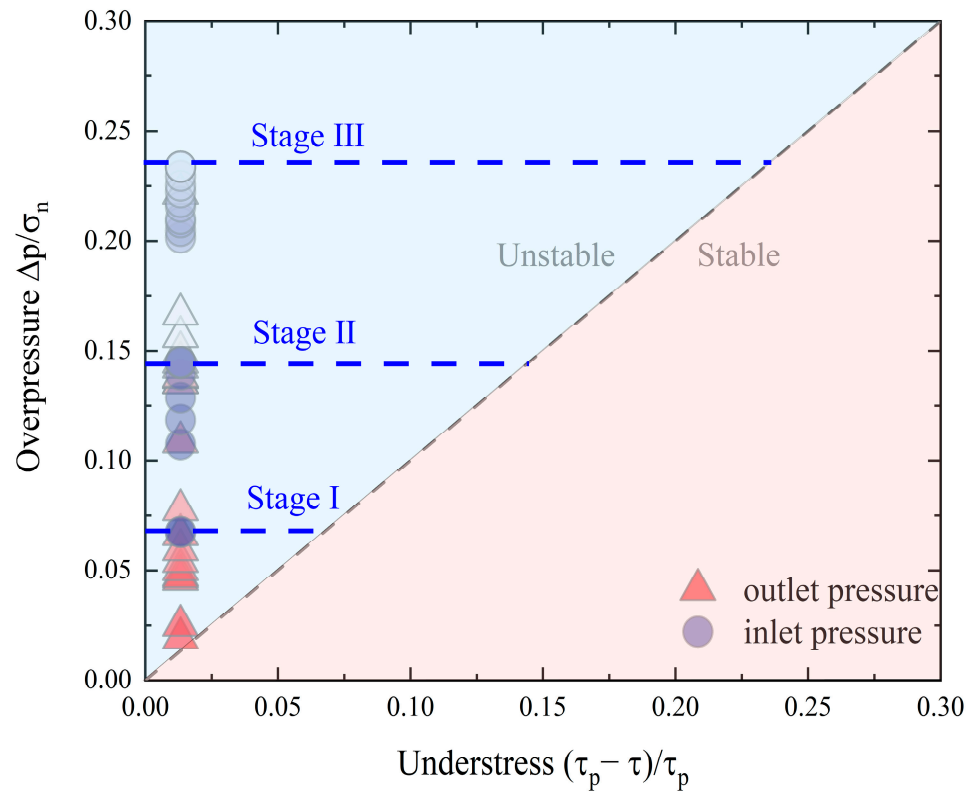


Figure 8. The overpressure and understress in the experiment.

4.2. Hydraulic Energy and Seismic Energy

To establish the relationship between input energy and output energy, the concept of hydraulic energy is adopted. The input and output energy can be described based on the conservation of energy. Therefore, the energy budget can be expressed using the following balanced formulation:

$$E_H + \Delta W = E_f + E_R + E_d + l \tag{6}$$

where E_H is the injected hydraulic energy, defined as the product of the injection fluid pressure (P Pa/s) and the injection rate (Q m³/s) (Equation (7)) [29]. The injected volume and pressure change with time. Thus, the injection energy is calculated by integrating E_H over the injection interval ($t_1 - t_2$). ΔW is the potential elastic energy. E_f is the frictional energy dissipated on the fault plane and is supposed to be equal to ΔW [30]. E_r is radiated energy, which is also regarded as seismic energy. It is hard to monitor the radiated energy because of the limited knowledge of the radiation pattern and limited frequency band [31]. Thus this energy is calculated by establishing the relationship [32] with the seismic moment (Equation (8)). E_d is deformation energy; l is energy loss, ignored in this experiment.

$$E_H = \int_{t_1}^{t_2} PQdt \tag{7}$$

$$\log_{10}(E_R) = 1.5M_w + 4.8 \tag{8}$$

According to Equation (6), each seismic event has a certain hydraulic energy (E_H) and radiated energy (E_r). The moment magnitude (M_w) can be calculated according to Equation (8). Therefore, the seismic energy (M_0) can be calculated according to Equation (4). Above this, the relationship between seismic energy and hydraulic energy is established. In Figure 9, the black line is the ratio between seismic energy and hydraulic energy. The 11 black lines represent the ratio of 100% to 0.00000001%, correspondingly. The triangles and circles in Figure 9 are data collected from several field experiments and laboratory

experiments. Therefore, Figure 9 shows the relationship between seismic energy and hydraulic energy. The triangle symbols represent the triggered seismicity and the circle symbols represent the induced seismicity. The total input hydraulic energy is 2.52 J. The deformation energy, aiming to enlarge the fracture aperture, ranges from 88% to 93% of the injection energy. Fluid could flow along the aperture more smoothly after several slips. The ratio of seismic energy and hydraulic energy is defined as seismic efficiencies. For triggered seismicity, the seismic efficiency ranges from 0.1% to 10%, referencing the field tests and laboratory tests. But for the induced seismicity, this parameter ranges from $1 \times 10^{-7}\%$ to $1 \times 10^{-3}\%$. According to Equation (7), we can deduce that the tectonic stress of a fracture and the fluid flow inside the fracture determines the released seismic energy. Therefore, seismic energy could be predicted using hydraulic energy.

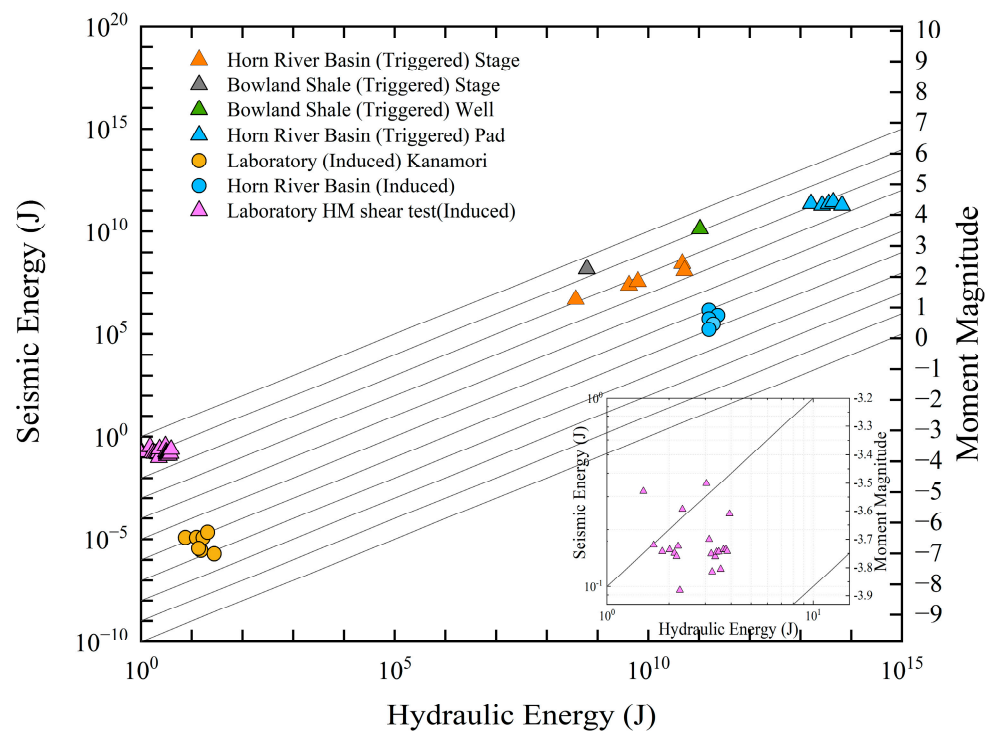


Figure 9. The injection energy is plotted against the seismic energy and moment magnitude.

5. Conclusions

This article concentrates on how fluid overpressure triggers the fracture slip by using the HM coupling shear test. A granite sample with a smooth fracture is adopted in this research. The injected water pressure increased cyclically to simulate water reservoir impoundment. During the test, stick-slip happens correspondingly to the inlet and outlet pressure. The HM coupling shear test shows that the fracture becomes unstable while the fluid pressure increases to a critical value. Cyclic water pressurization is introduced in this experiment. Results show that the fracture begins to slip when both the inlet and outlet pressure exceeds the theoretical water pressure and continues to stick-slip when both the inlet and outlet pressure increase. The slip distance, slip rate, and stress drop indicate that stick-slips happen periodically. The motivation for fracture sliding is the unbalance between the inlet pressure and outlet pressure, driving the fracture to become unstable. When the new balance between the inlet and outlet pressure has formed, the pressure-controlled stick-slip will turn into a stable sliding state. In addition, the fracture surfaces become deteriorated after several stick-slips for the RMS alteration after sliding. The understress is defined to explain the mechanism of fracture activation. The values of $\Delta p/\sigma_n$ and $1 - r_c$ determine the sliding state. When $\Delta p/\sigma_n < 1 - r_c$, the increased pressure and shear stress cannot induce slip. When $\Delta p/\sigma_n > 1 - r_c$, the fault is transitioning from a stable state to an unstable state. Furthermore, hydraulic energy is adopted as another

explanation as to why fluid overpressure can induce unstable sliding by establishing the relationship between the input energy and the released energy. Based on this, the seismic energy can be estimated from the input hydraulic energy, which is an effective method for evaluating reservoir-induced seismicity. Going forward, future work is required to determine why seismic turns to aseismic while the new balance is formed, which is also a complicated problem in predicting the magnitude of seismicity.

Author Contributions: Conceptualization, Y.Z. and C.X.; methodology, Y.Z.; validation, Y.Z. and C.X.; investigation, Y.Z. and X.L.; resources, X.L.; data curation, D.S.; writing—original draft preparation, Y.Z.; writing—review and editing, X.L. and E.W.; supervision, X.L. and E.W.; funding acquisition, Y.Z. and C.X. All authors have read and agreed to the published version of the manuscript.

Funding: This research was funded by the Open Research Fund Program of State key Laboratory of Hydrosience and Engineering (sklhse-2022-D-01, sklhse-2022-C-04), the Natural Science Foundation of Hubei Province, China (2022CFB673).

Data Availability Statement: Not applicable.

Conflicts of Interest: The authors declare no conflict of interest.

References

1. Elsworth, D.; Spiers, C.J.; Niemeijer, A.R. Understanding induced seismicity. *Science* **2016**, *354*, 1380–1381. [[CrossRef](#)]
2. Baker, J.; Ellsworth, W.; Beroza, G.; Schultz, R. Risk-Informed Recommendations for Managing Hydraulic Fracturing–Induced Seismicity via Traffic Light Protocols. *Bull. Seismol. Soc. Am.* **2020**, *110*, 2411–2422. [[CrossRef](#)]
3. Fang, Y.; den Hartog, S.A.M.; Elsworth, D.; Marone, C.; Cladouhos, T. Anomalous distribution of microearthquakes in the Newberry Geothermal Reservoir: Mechanisms and implications. *Geothermics* **2016**, *63*, 62–73. [[CrossRef](#)]
4. Sibson, R.H. Earthquake Rupturing in Fluid-Overpressured Crust: How Common? *Pure Appl. Geophys.* **2014**, *171*, 2867–2885. [[CrossRef](#)]
5. Sibson, R.H. Brittle-failure controls on maximum sustainable overpressure in different tectonic regimes. *AAPG Bull.* **2003**, *87*, 901–908. [[CrossRef](#)]
6. Sibson, R.H. Controls on maximum fluid overpressure defining conditions for mesozonal mineralisation. *J. Struct. Geol.* **2004**, *26*, 1127–1136. [[CrossRef](#)]
7. Nn, A.; Hs, B.; Ku, A. Fluid overpressure in subduction plate boundary caused by mantle-derived fluids—ScienceDirect. *Earth Planet. Sci. Lett.* **2020**, *538*, 116199.
8. Cappa, F.; Scuderi, M.M.; Collettini, C.; Guglielmi, Y.; Avouac, J.-P. Stabilization of fault slip by fluid injection in the laboratory and in situ. *Sci. Adv.* **2019**, *5*, eaau4065. [[CrossRef](#)]
9. Moernaut, J.; Wiemer, G.; Reusch, A.; Stark, N.; Batist, M.D.; Urrutia, R.; Bruno, L.; Kopf, A.; Strasser, M. The influence of overpressure and focused fluid flow on subaquatic slope stability in a formerly glaciated basin: Lake Villarrica (South-Central Chile). *Mar. Geol.* **2017**, *383*, 35–54. [[CrossRef](#)]
10. Tingay, M.R.P.; Hillis, R.R.; Swarbrick, R.E. Origin of overpressure and pore-pressure prediction in the Baram province, Brunei. *AAPG Bull.* **2009**, *93*, 51–74. [[CrossRef](#)]
11. Liu, Y.; He, Z.; He, S.; Zhang, D.; Li, T.; Wang, X. A new quantitative model and application for overpressure prediction in carbonate formation. *J. Pet. Sci. Eng.* **2021**, *198*, 108145. [[CrossRef](#)]
12. Yujie, Z.; Xiaoli, L.; Enzhi, W. Influence of impoundment gravity and pore pressure on reactivation of faults. *Geomech. Geophys. Geo-Energy Geo-Resour.* **2020**, *6*, 64. [[CrossRef](#)]
13. Ye, Z.; Ghassemi, A. Injection-Induced Shear Slip and Permeability Enhancement in Granite Fractures. *J. Geophys. Res. Solid Earth* **2018**, *123*, 9009–9032. [[CrossRef](#)]
14. Dugan, B.; Flemings, P.B. Overpressure and fluid flow in the new jersey continental slope: Implications for slope failure and cold seeps. *Science* **2000**, *289*, 288–291. [[CrossRef](#)]
15. Gudmundsson, A. Fluid overpressure and stress drop in fault zones. *Geophys. Res. Lett.* **1999**, *26*, 115–118. [[CrossRef](#)]
16. Osborne, M.J.; Swarbrick, R.E. Mechanisms for Generating Overpressure in Sedimentary Basins: A Reevaluation. *AAPG Bull.* **1997**, *81*, 1023–1041.
17. Noël, C.; Passelègue, F.X.; Giorgetti, C.; Violay, M. Fault Reactivation During Fluid Pressure Oscillations: Transition From Stable to Unstable Slip. *J. Geophys. Res. Solid Earth* **2019**, *124*, 10940–10953. [[CrossRef](#)]
18. Bell, M.L.; Nur, A. Strength changes due to reservoir-induced pore pressure and stresses and application to Lake Oroville. *J. Geophys. Res.* **1978**, *83*, 4469–4483. [[CrossRef](#)]
19. Brown, M.R.M.; Ge, S. Distinguishing Fluid Flow Path from Pore Pressure Diffusion for Induced Seismicity. *Bull. Seismol. Soc. Am.* **2018**, *108*, 3684–3686. [[CrossRef](#)]
20. Derode, B.; Guglielmi, Y.; De Barros, L.; Cappa, F. Seismic responses to fluid pressure perturbations in a slipping fault. *Geophys. Res. Lett.* **2015**, *42*, 3197–3203. [[CrossRef](#)]

21. Ji, Y.; Wanniarachchi, W.A.M.; Wu, W. Effect of fluid pressure heterogeneity on injection-induced fracture activation. *Comput. Geotech.* **2020**, *123*, 103589. [[CrossRef](#)]
22. Noël, C.; Pimienta, L.; Violay, M. Time-Dependent Deformations of Sandstone During Pore Fluid Pressure Oscillations: Implications for Natural and Induced Seismicity. *J. Geophys. Res. Solid Earth* **2019**, *124*, 801–821. [[CrossRef](#)]
23. Scuderi, M.M.; Collettini, C.; Marone, C. Frictional stability and earthquake triggering during fluid pressure stimulation of an experimental fault. *Earth Planet. Sci. Lett.* **2017**, *477*, 84–96. [[CrossRef](#)]
24. Violay, M.; Nielsen, S.; Spagnuolo, E.; Cinti, D.; Di Toro, G.; Di Stefano, G. Pore fluid in experimental calcite-bearing faults: Abrupt weakening and geochemical signature of co-seismic processes. *Earth Planet. Sci. Lett.* **2013**, *361*, 74–84. [[CrossRef](#)]
25. Garagash, D.I.; Germanovich, L.N. Nucleation and arrest of dynamic slip on a pressurized fault. *J. Geophys. Res. Solid Earth* **2012**, *117*, B10. [[CrossRef](#)]
26. Gischig, V.S. Rupture propagation behavior and the largest possible earthquake induced by fluid injection into deep reservoirs. *Geophys. Res. Lett.* **2015**, *42*, 7420–7428. [[CrossRef](#)]
27. Dieterich, J.H. Time-dependent friction as a possible mechanism for aftershocks. *J. Geophys. Res.* **1972**, *77*, 3771–3781. [[CrossRef](#)]
28. Ruina, A. Slip instability and state variable friction laws. *J. Geophys. Res. Solid Earth* **1983**, *88*, 10359–10370. [[CrossRef](#)]
29. Goodfellow, S.D.; Nasser, M.H.B.; Maxwell, S.C.; Young, R.P. Hydraulic fracture energy budget: Insights from the laboratory. *Geophys. Res. Lett.* **2015**, *42*, 3179–3187. [[CrossRef](#)]
30. Kanamori, H.; Brodsky, E.E. The physics of earthquakes. *Rep. Prog. Phys.* **2004**, *67*, 1429–1496. [[CrossRef](#)]
31. Ide, S.; Beroza, G.C. Does apparent stress vary with earthquake size? *Geophys. Res. Lett.* **2001**, *28*, 3349–3352. [[CrossRef](#)]
32. Neda, B.; Eaton, D.W. Comparing energy calculations: Hydraulic fracturing and microseismic monitoring. In Proceedings of the 74th EAGE Conference and Exhibition Incorporating EUROPEC 2012, Copenhagen, Denmark, 4–7 June 2012.

Disclaimer/Publisher’s Note: The statements, opinions and data contained in all publications are solely those of the individual author(s) and contributor(s) and not of MDPI and/or the editor(s). MDPI and/or the editor(s) disclaim responsibility for any injury to people or property resulting from any ideas, methods, instructions or products referred to in the content.